Star-Shaped Crack Pattern of Broken Windows

Nicolas Vandenberghe,* Romain Vermorel,† and Emmanuel Villermaux‡
Aix-Marseille Université, IRPHE, 13384 Marseille, France
(Received 31 January 2013; published 26 April 2013)

Broken thin brittle plates like windows and windshields are ubiquitous in our environment. When impacted locally, they typically present a pattern of cracks extending radially outward from the impact point. We study the variation of the pattern of cracks by performing controlled transverse impacts on brittle plates over a broad range of impact speed, plate thickness, and material properties, and we establish from experiments a global scaling law for the number of radial cracks incorporating all these parameters. A model based on Griffith's theory of fracture combining bending elastic energy and fracture energy accounts for our observations. These findings indicate how the postmortem shape of broken samples are related to material properties and impact parameters, a procedure relevant to forensic science, archaeology, or astrophysics.

DOI: 10.1103/PhysRevLett.110.174302 PACS numbers: 46.50.+a, 46.70.De

Patterns of multiple cracks, such as those appearing on broken windows [1,2], remain difficult to interpret, because the crack extension and the inherent modification of the stress field are intertwined. These networks of cracks are, however, of prime importance to understand fragment size distributions resulting from impacts [3], a fundamental problem of interest for the crushing and grinding process industry. Studies addressing the behavior of a plate impacted by a projectile have been numerous in relation to security applications [4,5]. In this context the emphasis is usually put on the damage or perforation of armor plates made of high strength ductile materials, and different perforation mechanisms leading to different postmortem shapes have been identified [6,7]. Numerous studies have also addressed the case of brittle material such as glass and the difficult problem, even in static configurations [8], of determining thresholds for damage. We focus here on situations of dynamical impacts on brittle plates, and on the formation of radial cracks whose extension is in general much larger than the size of the impactor, and perform controlled transverse impact experiments on plates of PMMA poly(methyl methacrylate), a brittle plastic, and glass.

The plates of PMMA (Young's modulus $Y = 3.3 \times 10^9$ Pa, density $\rho = 1.19 \times 10^3\,\mathrm{kg\,m^{-3}}$, and Poisson ratio $\nu = 0.39$) have thicknesses h in the millimeter range ($h = 0.5$, 1.0, 1.5, and 3 mm) and side length of 15 cm. They are held on a square frame with magnets, and we focus on the response at short times for which the boundary conditions on the sides of the plate do not affect the dynamics. A steel cylinder of mass 16 g with a hemispherical end of radius $r_i = 1.8$ mm is accelerated with a gas gun. It impacts the plates perpendicularly at their center at speeds in the range 10–120 m/s. The plate surface is observed from the face opposite the impact and the dynamics is recorded with a high speed camera recording 30 000 frames per second.

After impact, the plate is deformed by a transverse bending wave growing in amplitude and radius. For speeds above a threshold (typically 15 m/s for $h = 1$ mm), a pattern of radial cracks is observed early in the dynamics (Fig. 1). In most cases, the number of cracks is set very early on ($t \leq 33$ μs after impact) and it does not vary as the radial cracks extend. Their angular distribution is quite regular, and at a given time all the cracks present approximately the same length. At later times, waves interact with the boundaries and the pattern loses its regularity. As we increase impact speed from 15 to 120 m/s, the number of cracks increases from 3 to 11. At low speeds (below 65 m/s for $h = 1$ mm), radial cracks extend until they reach the sides of the plate. At high impact speeds, the petals delimited by the radial cracks break to form circumferential cracks resembling the conical cracks characteristic of Hertzian fracture [8]. They appear at short times at radii comparable with the radius of the impactor. Different stages of circumferential cracks develop [Fig. 1(c)] together with radial cracks resulting in the formation of very small fragments. At higher speeds, a large number of small fragments (with a characteristic size smaller than plate thickness) are ejected. Typically, in this high speed regime, the impacted plate exhibits a hole the size of the impactor and thus the damaged area on the plate is smaller than at low impact speeds.

For the lower range of impact speeds, the pattern evolves in time. At short times two cracks extend out of the point of impact, until new cracks form [Fig. 2(a)]. This scenario is consistently observed at lower speeds for thin plates ($h = 0.5$, 1, or 1.5 mm). For thicker plates ($h = 3$ mm) we observe a reduction of the number of cracks when the pattern expands. As shown on Fig. 2(b), initially a large number of cracks form but only some of the cracks will expand to form well-delimited petals.

Experiments were also performed on thin glass slides ($Y = 6.1 \times 10^{10}$ Pa, $\rho = 2.38 \times 10^3\,\mathrm{kg\,m^{-3}}$, $\nu = 0.22$)

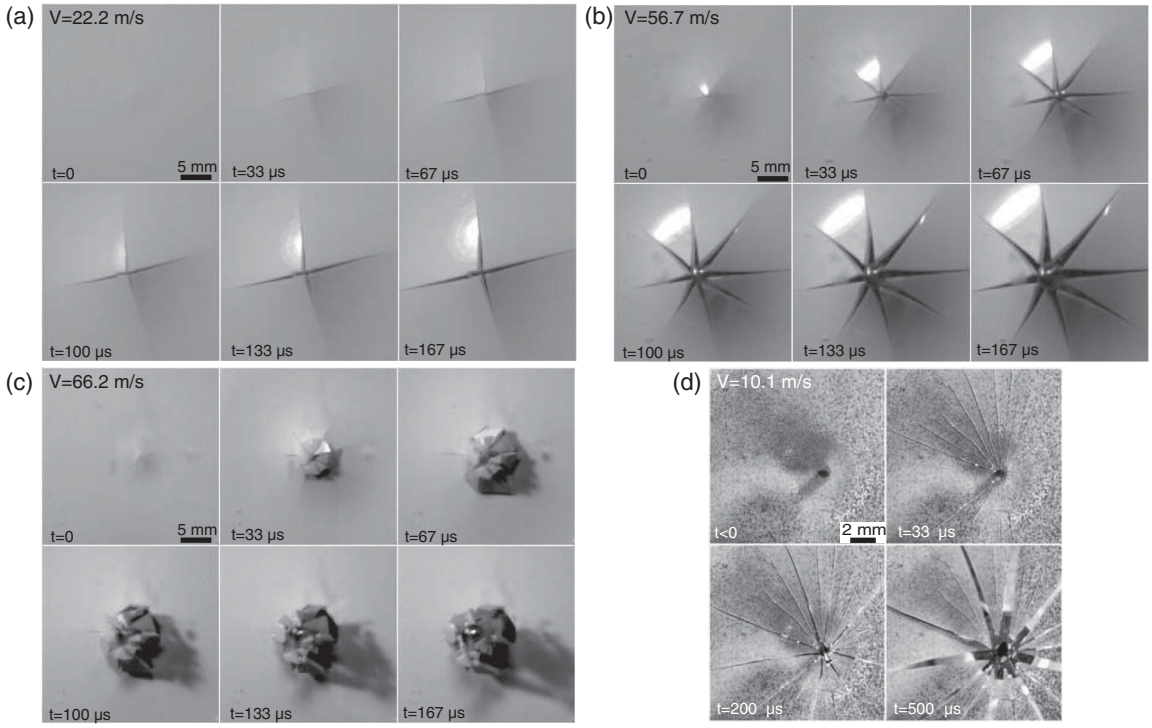

FIG. 1. Star-shaped crack patterns on impacted plates. PMMA plates of thickness $h = 1$ mm impacted transversely exhibit a pattern of radial cracks that extend until they reach the side of the plate (a), (b) while at higher speed (c) circumferential cracks characteristic of Hertzian fracture are also observed. (d) Similar patterns are observed on a glass slide of thickness $h = 0.15$ mm impacted at $V = 10.1$ m/s. One identifies numerous cracks on the first panel of which only 11 will appear as extending cracks on the other panels. For the purpose of visualization, white paint coats the glass plate.

with thickness $h = 0.15$ mm and side length 80 mm. The plates rest on an annulus of inner diameter 60 mm. The impactor is a cylinder of mass 3.3 g with a hemispherical end of radius $r_i = 0.5$ mm. At speeds in the range 5–40 m/s, we also observe patterns of radial cracks. After impact, a large number of cracks is apparent, but as the pattern extends, only some of them open and separate distinct petals [Fig. 1(d)].

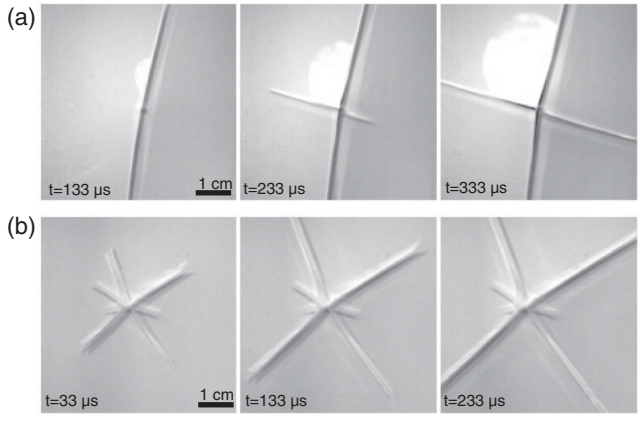

FIG. 2. Evolution of the crack pattern on impacted plates. (a) The augmentation of the number of cracks from 2 to 4 is typical of low speed impacts on thin plates (here PMMA with $h = 1.5$ mm). (b) For thicker plates (PMMA with $h = 3.0$ mm). Some of the cracks formed at short times do not extend (here 7 cracks are initially formed but only 4 of them extend.

The number of radial cracks of the final pattern for a given plate material shows a clear augmentation with the impact speed V and plate thickness h (Fig. 3). The number of radial cracks on PMMA plates of different thicknesses and of glass plates collapse when plotted against the non-dimensional speed $\hat{V} = (Eh/\Gamma)^{2/3}(V/c)$, where Γ is the fracture energy of the material (300 J/m^2 for PMMA and 3 J/m^2 for soda-lime glass, within the range of values in the literature [9,10]) and $c = (E/\rho)^{1/2}$ with $E = Y/(1-\nu^2)$ is the speed of sound in the material.

After contact with the plate, and after a short transient involving compression in the bulk of the plate lasting t_H, the impactor triggers bending waves [11]. Kinetic and bending energies balance, $\rho\Omega V^2 \sim E(\kappa h)^2\Omega$ with curvature $\kappa \sim w_0/r_f^2$, $w_0 = Vt$ the indentation, and r_f the radius of the deformed region (the volume of deformed material is $\Omega = \pi r_f^2 h$), yielding $r_f \sim (cht)^{1/2}$. The curvature $\kappa \sim V/(ch)$ is constant in time [12,13]. Energies have been estimated in a quasistatic fashion, time entering in the description through boundary conditions only, themselves a function of time. This implies that we consider time scales long with respect to the propagation time of the strain in the medium, and in particular to the smallest, based on the plate thickness $t_s = h/c$.

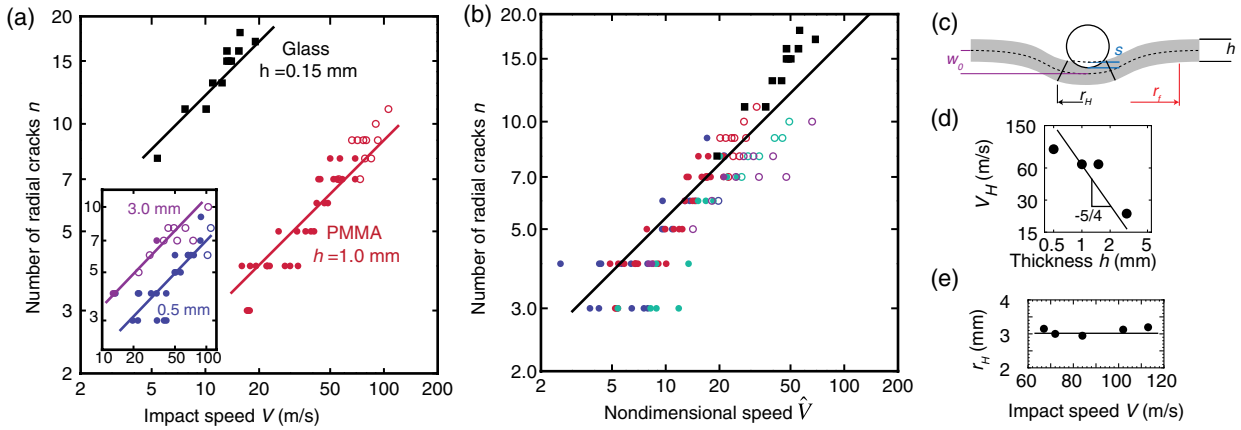

FIG. 3 (color online). Evolution of the pattern with impact speed. (a) The number of radial cracks increases with impact speed V for PMMA plates ($h = 1$ mm) and for glass slides ($h = 0.15$ mm). The lines are $n \sim V^{1/2}$. Inset: Number of radial cracks versus impact speed for PMMA plates of thickness 0.5 and 3.0 mm. (b) The results are conveniently rescaled using the nondimensional impact speed $\hat{V} = (Eh/\Gamma)^{2/3}(V/c)$. Impact experiments were performed on PMMA plates (●) with $h = 0.5$, 1.0, 1.5, 3.0 mm, and glass plates ($h = 0.15$ mm, ■). The continuous line is the scaling law in Eq. (3) with a prefactor equal to 1.7. Open symbols are for impacts presenting circumferential cracks. (c) The short time response consists of a deformation in the bulk and a bending deformation. (d) The impact speed V_H at which circumferential cracks appear decreases with plate thickness. (e) The radius of the first circumferential cracks is constant with V (for PMMA plates with $h = 1.5$ mm).

The bending response holds as soon as the compression energy stored at the contact of the impactor $E(Vt/r_H)^2 r_H^3$, with $r_H^2 = r_i Vt$ given by Hertz theory of contact [14,15], overcomes the bending energy $E(V/c)^2 r_f^2 h$ above. This occurs at $t_H \sim (h/c)(c/V)^{1/3}(h/r_i)^{1/3}$ larger than t_s since $V \ll c$. Comparing the stored elastic energy $E r_i^{1/2}(Vt_H)^{5/2}$ at t_H with the energy needed to expand circumferential cracks [16] across the plate $\Gamma h r_H$ yields a scaling law for the critical speed at which the circumferential cracks should appear $V \sim h^{-5/4}$ in agreement with observation [Fig. 3(d)]. The circumferential cracks appear at a radius r_H that does not depend on impact speed [Fig. 3(e)].

Finally, we note that the transverse deformation is accompanied by stretching through geometric nonlinearities. The stretching $\epsilon \sim (w_0/r_f)^2$ becomes significant when the stretching energy $E(w_0/r_f)^4 r_f^2 h$ becomes comparable with the bending energy, at time $t_f = h/V$.

The bending energy U_b of an elastic plate with transverse displacement $w(r, \theta)$ is

$$\frac{Eh^3}{24} \iint [\kappa_r^2 + \kappa_\theta^2 + 2\nu\kappa_r\kappa_\theta + 2(1-\nu)\kappa_{r\theta}^2] r dr d\theta, \quad (1)$$

where $\kappa_r = \partial_{rr} w$, $\kappa_\theta = (1/r)\partial_r w + (1/r^2)\partial_{\theta\theta} w$, $\kappa_{r\theta} = (1/r)\partial_{r\theta} w - (1/r^2)\partial_\theta w$. For a plate clamped at an outer radius r_f with n regularly spaced radial cracks which extends to ξr_f (with $\xi < 1$), the gain in elastic energy that is inherent to crack extension is mainly due to the flattening of the petals in the orthoradial direction and the corresponding reduction of the bending energy associated with the curvature κ_θ. Indeed, near $r = 0$, the impact response of a plate [13] yields $(\kappa_\theta - \kappa_r)/\kappa_\theta \sim -(8/\pi)/\log(r/r_f)$ and radial cracks are arguably favored since $|\kappa_\theta| > |\kappa_r|$.

We perform indentation experiments of thin polycarbonate plate ($Y = 2.3 \times 10^9$ Pa, $\nu = 0.35$, $h = 1$ mm) clamped at an outer radius $r_f = 60$ mm, on which n radial cuts extending to ξr_f (with $\xi < 1$) were made with a thin (0.2 mm wide) saw blade, measuring the force F to achieve indentation w_0, thus inferring elastic energy $U_b = F w_0/2$. The result is a parabolic relationship (for displacement less than 1 mm) with a coefficient U_b/w_0^2 which can be used to compute the stiffness of the cracked plate $k_b(\xi, n) = (U_b/w_0^2)(3r_f^2/\pi E h^3)$.

These results can be accounted for by a low-dimensional model. We consider two domains in the plate: first, an outer domain ($r > \xi r_f$) which is uncut, where the displacement is taken as the displacement for an unbroken circular plate loaded at its center [17] $f_e(r) = \alpha[1 - (r/r_f)^2 + 2(r/r_f)^2 \log(r/r_f)]$. In the inner domain, we add a non-axisymmetric displacement for the petals $r < \xi r_f$. For the petal bounded by cracks at $-\pi/n$ and π/n, the displacement is of the form $w_i(r, \theta) = f_e(r) + (1 - \alpha - \beta x)(1 - x^2)$, with $x = (r/\xi r_f)\cos\theta/\cos(\pi/n)$. Using this ansatz for the displacement w, we construct the bending energy. The two parameters α and β are then obtained by minimizing the bending energy, giving $k_b(1, n) \approx 0.46 + 2.8/n^2$. We obtain a good agreement between this simple model and our measurements, thus indicating that the flattening of the petals is a key element to understand how the cuts alter the bending rigidity of the plate [Fig 4(c)]. Bending energy is minimal when cracks are extended ($\xi \to 1$). In this

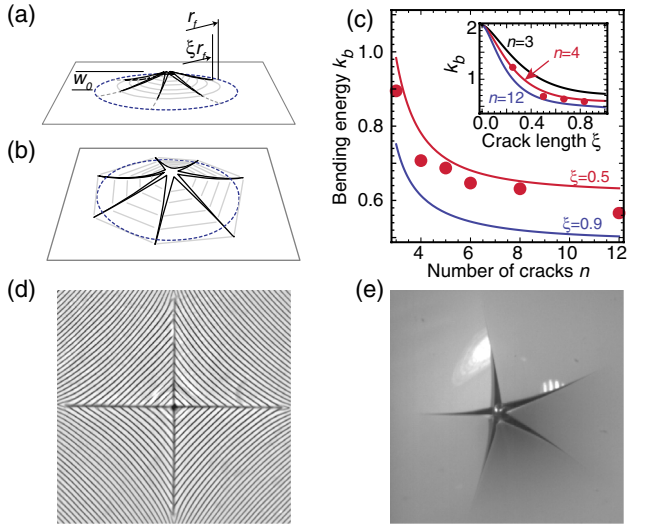

FIG. 4 (color online). Bending of a cracked plate. (a) The wave front is located in r_f, crack tips at ξr_f, and the impactor is at w_0. (b) When the cracks have reached the position $r_f/\cos(\pi/n)$, the petals are flat in their transverse direction. (c) The nondimensional bending energy $k_b = U_b 3r_f^2/(\pi E h^3 w_0^2)$ of a clamped plate presenting n radial cracks decreases with n and with the crack length ξ (inset). The lines are obtained from theory and the dots are experimental points obtained on a 1 mm thick polycarbonate plate with radial cuts made with a thin blade. (d) Squares reflected in a bent plate with 4 cracks show that, close to the center, reflected lines are almost straight and thus petals flatten near the center. (e) An impacted plate exhibits petals that are flat near the impact point.

configuration, the energy can be estimated, neglecting transverse bending, by the energy of n triangular beams. The bending energy of n triangular beams of length r_f and summit angle $2\pi/n$ is $Eh^3 w_0^2 n \tan(\pi/n)/(3r_f^2)$ and thus $k_b(1, n) \approx 1/2 + \pi^2/(6n^2)$.

In Griffith's theory of brittle fracture [18], the pattern of cracks corresponds to the global energy (i.e., elastic plus fracture) minimum [19–22]. Using the bending energy previously computed in the limit of long cracks extending up to $r_f/\cos(\pi/n)$ (optimization could be performed on ξ as well, leading to no significant difference) and the fracture energy $2n\Gamma h r_f$, the total energy can be written as

$$E\frac{\pi r_f^2 h}{3}\left(\frac{w_0 h}{r_f^2}\right)^2\left\{\frac{1}{2}+\frac{\pi^2}{6n^2}\right\} + 2n\Gamma h r_f, \qquad (2)$$

with Γ the material fracture (surface) energy. Minimizing with respect to n, with $w_0 = Vt$, the optimal number of cracks is $n \sim (Er_f/\Gamma)^{1/3}(V/c)^{2/3}$. There are more cracks in more brittle material (lower Γ), impacted more violently (higher V). The number n is also anticipated to increase (slowly) with time, through $r_f \sim (cht)^{1/2}$. This is consistent with Fig. 2, but at some point the increase stops and the pattern is frozen.

The freezing time, after which a global energy minimization loses its sense, corresponds to the end of the elastic connectivity of the pattern. The orthoradial curvature of a petal is released when the crack tip has reached $r_f/\cos(\pi/n)$. To drive the crack up to this point, transverse displacement must occur in the area between r_f and $r_f/\cos(\pi/n)$. This is not possible as long as wave propagation results solely from the balance between kinetic and bending energy. Stretching can drive the transverse wave farther than r_f. Stretching energy $E(Vt/r_f)^4\Omega$ dominates bending energy $E(V/c)^2\Omega$ for times larger than $t_f = h/V$. At that time, the number of cracks is, and will remain

$$n \sim \left(\frac{Eh}{\Gamma}\right)^{1/3}\left(\frac{V}{c}\right)^{1/2}, \qquad (3)$$

explaining the scaling $n = 1.7\hat{V}^{1/2}$ as seen in Fig. 3.

The study of patterns resulting from impact is a valuable source of information on past or distant events in different fields [23–25]. Our results reveal that quantitative insights on the nature of the impacted sample and on the impact conditions can be obtained from the number of radial cracks. In astrophysics, impact patterns, either natural or man made, are a means of investigation to infer properties of distant bodies [26]. Though thin layers of brittle materials are often encountered on various planets, these always lie on a soft or fluid substrate. Finally, we note the similarity between the patterns resulting from impacts and the patterns observed on brittle coatings on soft substrate [27]. In particular, the coexistence of radial and circumferential cracks is observed in both cases and the evolution of the number of cracks with indentation load has been observed [28]. In these analogous situations, the crack pattern is constrained by an intrinsic length scale, characterizing the radial extension of the deformed area, evolving with time in the case of impact (like r_f), and which is equal to $(Eh^3/12k)^{1/4}$, where k is the modulus of the foundation [17] in the case of static indentation of brittle coatings.

We acknowledge support from the Agence Nationale de la Recherche through Grants No. ANR-05-BLAN-0222-01 and No. ANR-11-JS09-0005 and from the Direction Générale de l'Armement.

*vandenberghe@irphe.univ-mrs.fr
†Present address: Université de Pau, LFC-R, 64013 Pau, France.
‡Also at Institut Universitaire de France, 75005 Paris, France.

[1] N. Shinkai, in *Fractography of Glass*, edited by R. C. Bradt and R. E. Tressler (Plenum, New York, 1994).
[2] J. Åström and J. Timonen, Phys. Rev. Lett. **79**, 3684 (1997).
[3] D. Grady, *Fragmentation of Rings and Shells* (Springer-Verlag, Berlin, 2006).

[4] M. A. Backmann and W. Goldsmith, Int. J. Eng. Sci. **16**, 1 (1978).
[5] G. Corbett, S. Reid, and W. H. Johnson, Int. J. Impact Eng. **18**, 141 (1996).
[6] T. Wierzbicki, Int. J. Impact Eng. **22**, 935 (1999).
[7] A. Atkins, Int. J. Impact Eng. **21**, 521 (1998).
[8] B. Lawn, *Fracture of Brittle Solids* (Cambridge University Press, Cambridge, England, 1993), 2nd ed.
[9] F. G. Katsamanis and C. G. Delides, J. Phys. D **21**, 79 (1988).
[10] K. R. Linger and D. G. Holloway, Philos. Mag. **18**, 1269 (1968).
[11] C. Zener, Phys. Rev. **59**, 669 (1941).
[12] J. Boussinesq, *Application des Potentiels à l'étude de l'équilibre et du Mouvement des Solides Élastiques* (Gauthier-Villars, Paris, 1885).
[13] K. F. Graff, *Wave Motion in Elastic Solids* (Dover, New York, 1975).
[14] H. Hertz, *Miscellaneous Papers* (McMillan and Co., London, 1882), pp. 146–162.
[15] L. D. Landau and E. M. Lifshitz, *Theory of Elasticity*, Course of Theoretical Physics Vol. 7 (Pergamon, Oxford, England, 1986), 3rd ed.
[16] F. Roesler, Proc. Phys. Soc. London Sect. B **69**, 55 (1956).
[17] A. E. H. Love, *A Treatise on the Mathematical Theory of Elasticity* (Dover, New York, 1944), 4th ed.
[18] A. Griffith, Phil. Trans. R. Soc. A **221**, 163 (1921).
[19] G. Francfort and J. Marigo, J. Mech. Phys. Solids **46**, 1319 (1998).
[20] G. Gauthier, V. Lazarus, and L. Pauchard, Europhys. Lett. **89**, 26 002 (2010).
[21] Z. P. Bazant and Y. Li, Int. J. Solids Struct. **32**, 303 (1995).
[22] R. Vermorel, N. Vandenberghe, and E. Villermaux, Phys. Rev. Lett. **104**, 175502 (2010).
[23] J. Locke and J. A. Unikowski, Forensic Sci. Int. **51**, 251 (1991).
[24] H. Shin, C. Doumas, T. Funkhouser, S. Rusinkiewicz, K. Steiglitz, A. Vlachopoulos, and T. Weyrich, J. Comput. Cult. Heritage **5**, 10 (2012).
[25] H. J. Melosh, *Impact Cratering: A Geologic Process* (Oxford University Press, Oxford, England, 1989).
[26] E. Turtle and E. Pierazzo, Science **294**, 1326 (2001).
[27] B. R. Lawn, J. J. W. Lee, and H. Chai, Annu. Rev. Mater. Res. **40**, 55 (2010).
[28] H. Chai, B. R. Lawn, and S. Wuttiphan, J. Mater. Res. **14**, 3805 (1999).